npj | Materials Degradation

www.nature.com/npjmatdeg

ARTICLE OPEN

Sub-stoichiometry-facilitated oxidation kinetics in a δ-Ti_xC-doped Ti-based alloy

Shaolou Wei[1,2], Lujun Huang[1], Yuntong Zhu[2], Zhe Shi[2], Xinting Li[1] and Lin Geng[1]

Titanium carbide has been widely considered as a stabilizer to alleviate the serious chemical activity of Ti-based alloys at elevated temperatures. However, a reverse effect may also take place: we show the sub-stoichiometry characteristic of δ-Ti_xC can facilitate the oxidation kinetics of a Ti-6Al-4V alloy to a significant extent. In particular, oxygen atoms tend to preferentially occupy the vacant carbon sites within the Ti_2C phase, giving rise to a higher oxidation rate. The intrinsic mechanisms were understood with a combination of ab initio simulation and experimental validation.

npj Materials Degradation (2019)3:3 ; https://doi.org/10.1038/s41529-018-0067-9

INTRODUCTION

Transition metal carbides have aroused remarkable research interest owing to the unique combination of high melting point, superior hardness, and excellent thermal conductivity.[1–3] In terms of crystal structure, the most intriguing characteristic is the existence of prevalent carbon vacancies within the Fm-3m (B1-NaCl) prototypical lattice.[4,5] An abundance of experimental and theoretical efforts have evidenced the linkage between vacancy concentration and fluctuations in bulk properties such as hardness, chemical stability, and electric conductivity.[4,6–8] Recent literature also reflects attempts to construct the phase equilibrium framework via ab initio simulation.[9,10]

Amongst these group IV–V metal carbides, more attention has been directed to titanium carbide, namely, the δ-Ti_xC phase. On the one hand, the large degree of freedom in carbon stoichiometry of δ-Ti_xC ($1 < x < 2$) has stimulated broad theoretical interest in exploring the variation in equilibrium geometry, energy band structure, charge density distribution, and stacking fault energy with respect to the vacancy concentration.[11–14] On the other hand, the relatively high specific strength, desirable catalytic behavior, and favorable affinity with hydrogen have also enabled δ-Ti_xC to become extensively popular in both structural[15–18] and functional materials research.[19–22] In particular, δ-Ti_xC has been widely considered as a sort of stabilizer for Ti-based alloys to mitigate their strong oxidation propensity at elevated temperatures.[23,24]

Based on the kinetic features, current investigations of high-temperature-oxidation for metallic-based materials can be categorized into two types[25]: the first type of study explores the diffusion and adsorption characteristics of oxygen in the substrate lattice; the goal of the second type is to clarify compositional and structural evolution mechanisms for the oxidized substrate. With regard to Ti-based alloys or composites, an extensive amount of work has been accomplished toward the second type.[24,26–28] In particular, the positive contribution of δ-Ti_xC has been widely highlighted, as it can fasten the oxide scales by alleviating thermal mismatch.[24,29] In contrast, comparatively limited work found in the literature focuses on the motion of oxygen atoms within the Ti lattice.[30,31] So far, little attention has been paid to the influence of sub-stoichiometry on the oxidation behavior of δ-Ti_xC-containing Ti-based alloys and a gap still exists in our understanding of microscopic crystal defects and how they affect macroscopic oxidation kinetics.

In the present work, we have clarified the role of sub-stoichiometry in the oxidation kinetics of a δ-Ti_xC-doped Ti-based alloy via a combination of ab initio simulation and experimental verification. In contrast to the common interpretation of "δ-Ti_xC as a stabilizer", our results reveal that the sub-stoichiometry nature of δ-Ti_xC can facilitate the oxidation kinetics to a significant extent. In addition to their theoretical values to contribute to a more comprehensive understanding of oxidation mechanisms, these findings are of equal significance to guide high-temperature metallic or ceramic-based materials design.

RESULTS AND DISCUSSION

To theoretically understand the interactive effect of carbon vacancy and oxygen atoms at elevated temperatures, TiC (Fm-3m), Ti_2C (Fd3m), and α-Ti (P63/mmc) supercells each with 32 Ti atoms were constructed as illustrated in Fig. 1a. The energy variation after an oxygen atom occupies the interstices in TiC (tetrahedral site), Ti_2C (octahedral vacant carbon site), and α-Ti (octahedral site) is shown in Fig. 1c. At 873 K, the carbon-deficient Ti_2C exhibits the most remarkable energy decrease of 9.62 eV (2.27 %), which is almost eight times higher than that of the stoichiometric TiC (1.14 eV, 0.19 %). Such a significant discrepancy in energy variation results from the replacement of C–O bonds in TiC with even stronger Ti–O bonds in Ti_2C, as revealed in the differential charge density plot (Fig. 1b). Comparing the energy decrease of Ti_2C (9.62 eV, 2.27%) with α-Ti (8.65 eV, 1.76%), it is noteworthy that oxygen occupancy at the vacant carbon site is more energetically favorable, indicating a stronger oxidation tendency. In contrast to the prevalent understanding, these simulation results imply the following two new concepts: (1) instead of mitigating the oxidation rate, the carbon-deficient Ti_2C is expected to facilitate the oxidation kinetics when

[1]School of Materials Science and Engineering, Harbin Institute of Technology, Harbin 150001, P. R. China and [2]Department of Materials Science and Engineering, Massachusetts Institute of Technology, Cambridge, MA 02139, USA
Correspondence: Lujun Huang (huanglujun@hit.edu.cn) or Lin Geng (genglin@hit.edu.cn)

Received: 13 August 2018 Accepted: 17 December 2018
Published online: 11 January 2019

Published in partnership with CSCP and USTB

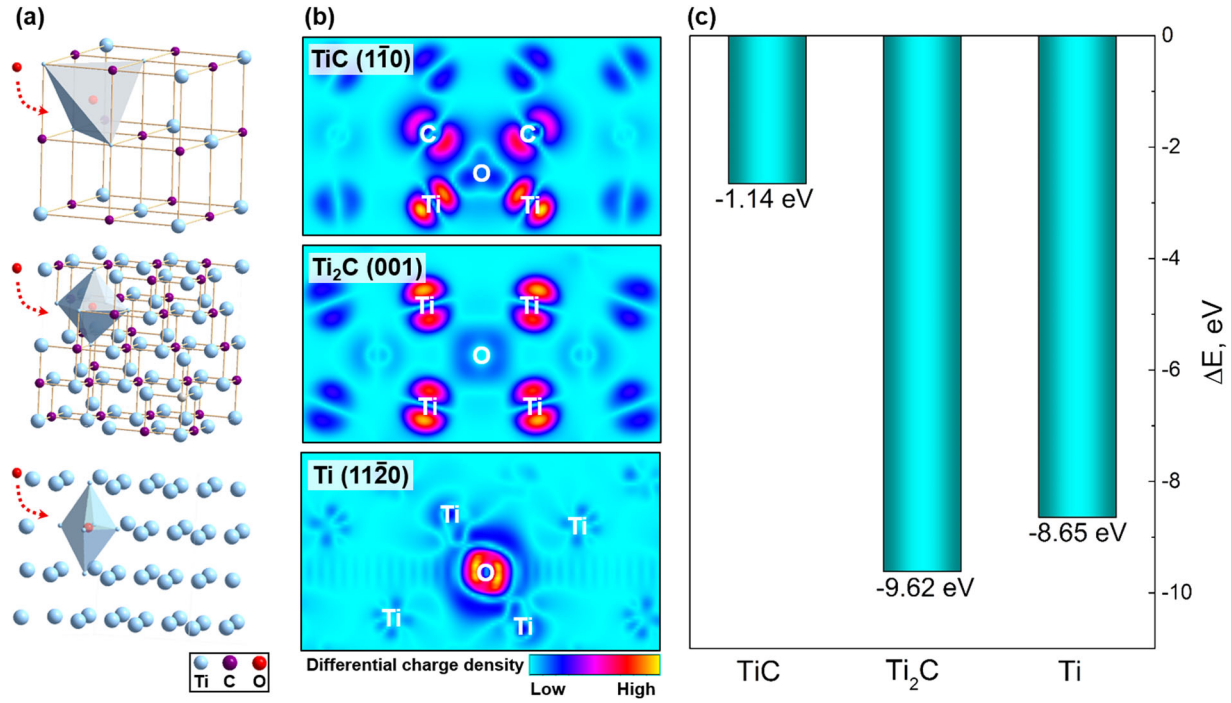

Fig. 1 Ab initio simulation of oxygen atom occupancy in TiC, Ti_2C, and α-Ti at 873 K: **a** configurations of oxygen atom occupancy, from top to bottom: tetrahedral site in TiC, octahedral vacant carbon site in Ti_2C, and octahedral site in α-Ti; **b** differential charge density plots; **c** energy variation after oxygen atom occupancy

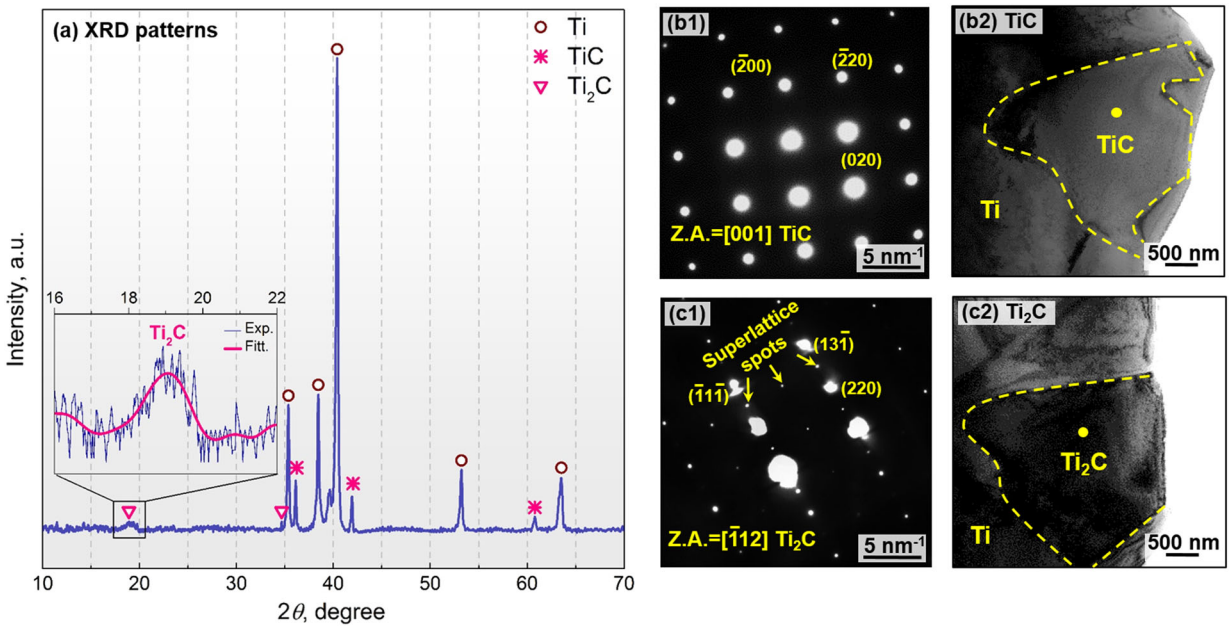

Fig. 2 Structural characterization of the δ-Ti_xC-doped Ti-6Al-4V alloy: **a** XRD patterns; **b**1 and **c**1 SAED patterns for TiC and Ti_2C; **b**2 and **c**2 corresponding TEM bright field images

doped into an α-Ti-based alloy; and (2) owing to the energetically favored oxygen occupancy at the ordered carbon vacancies, Ti_2C is supposed to exhibit a higher propensity for oxidization than its stoichiometric counterpart.

To examine the concepts proposed above, the most widely investigated Ti-6Al-4V/Ti_xC system was employed to experimentally investigate the oxidation kinetic features. Fig. 2 presents the phase constitutions and crystallographic analyses of the Ti_xC-doped Ti-6Al-4V alloy. The X-ray powder diffraction (XRD) patterns in Fig. 2a verify the existence of both TiC and Ti_2C phases. The characteristic diffraction peaks of Ti_2C appear at ~19° and 34°, agreeing well with the simulation results (supporting information) and similar work reported by Liu et al.[32] Selected area electron diffraction patterns clearly reveal the intrinsic distinctions in lattice structures: Fig. 2b1 displays typical perfect B1-type patterns corresponding to the [100] zone axis, which coincides with the results reported in the literature.[17] While in Fig. 2c1, <1/2, 1/2, 1/2> type superlattice spots can be clearly observed, and this

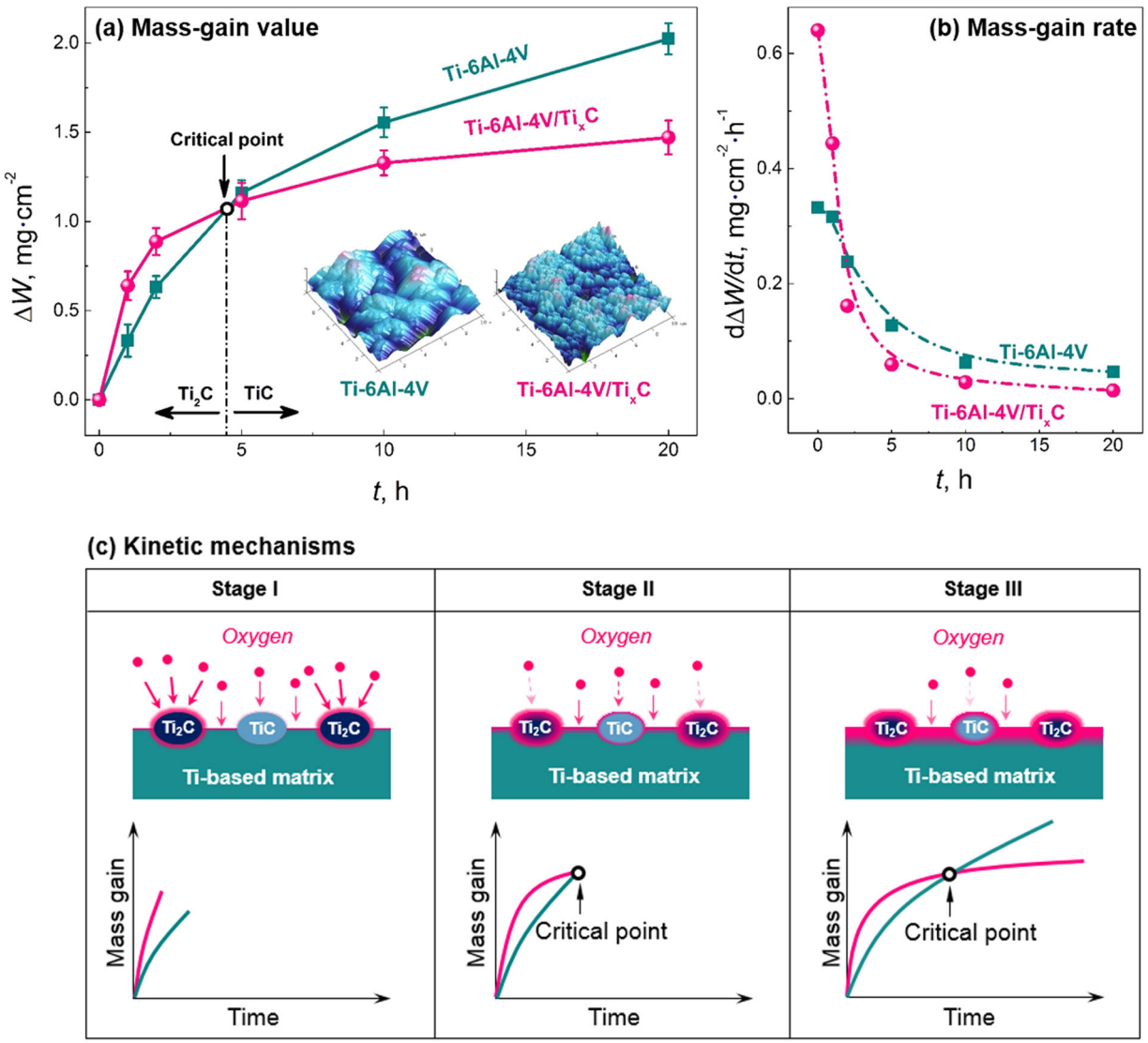

Fig. 3 Oxidation kinetics of the Ti-6Al-4V/Ti$_x$C and the monolithic Ti-6Al-4V alloys at 873 K: **a** mass-gain value (error bars denote standard deviation of five tested specimens); **b** mass-gain rate; **c** schematics for kinetic mechanisms

directly supports the existence of ordered micro-domains induced by the carbon vacancies. Compared with the previous work reported by Bursik et al.,[33] it can be concluded that the corresponding Ti/C ratio is 2, which is consistent with the XRD results. It should also be noted that no other types of superlattice spots are detected in the present investigation. As confirmed by the transmission electron microscope (TEM) bright-field analyses (Fig. 2b2 and c2), both TiC and Ti$_2$C bond well with the adjacent Ti matrix. No traits of interfacial reactions are observed.

Figure 3 demonstrates the oxidation kinetics of the Ti$_x$C-doped Ti-6Al-4V alloy and the monolithic one at 873 K. Consistent with the ab initio predictions, the Ti-6Al-4V/Ti$_x$C alloy exhibits a remarkably high mass-gain kinetics compared with its monolithic counterpart at the initial stage (Fig. 3a). The corresponding mass-gain rate of the Ti$_x$C-doped Ti-6Al-4V alloy exceeds 0.6 mg cm^{-2} h^{-1}, which is almost two times faster than that of the monolithic one (Fig. 3b). Interestingly, a kinetic critical point at ~4.8 h is also observed in Fig. 3a. According to the ab initio simulation results, this phenomenon is mostly attributed to the consumption of the Ti$_2$C phase (schematically depicted in Fig. 3c). In other words, owing to the energetically favored oxygen occupancy, the Ti$_2$C phase is preferentially oxidized at the very initial stage, expediting the mass-gain kinetics before the critical point (stage I in Fig. 3c). However, after the majority Ti$_2$C phase was oxidized, the following threefold mechanisms account for the decreased mass-gain rate (stages II and III in Fig. 3c). First, the rest of the Ti-6Al-4V/Ti$_x$C system is comparatively similar to Ti-6Al-4V/TiC where the stoichiometric TiC phase alleviates the high chemical activity of the Ti-based matrix. Second, the oxidized Ti$_2$C phase brings about the formation of thermodynamically stable TiO_2, acting as a localized passivation layer to suppress further oxidation. Third, the Ti$_2$C phase also has a role as heterogeneous nuclei for the oxides that gives rise to much denser and finer oxide scales, as seen in the inserted atomic force microscope (AFM) micrographs in Fig. 3a.

To further validate the proposed mechanisms, scanning electron microscope (SEM)/energy dispersive spectrometer (EDS) analyses were conducted in the Ti$_x$C-doped Ti-6Al-4V alloy specimen oxidized for 5 h. Four 1 μm^2 regimes (marked in Fig. 4a, b) were subjected to compositional analyses so as to eliminate the possible off-sets of EDS measurement. As summarized in Fig. 4c, the oxygen content in stoichiometric TiC is lower than that of its neighboring Ti matrix. On the contrary, Ti$_2$C exhibits a remarkably high oxygen content compared with the adjacent Ti matrix. It is recognized that these findings again confirm the ab

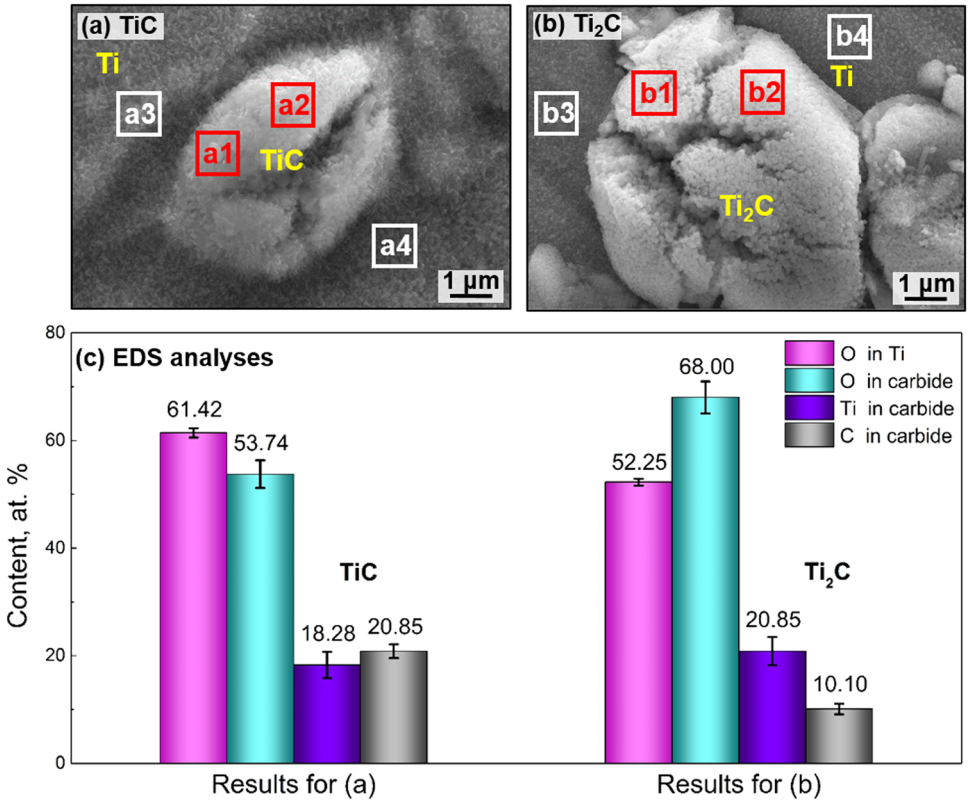

Fig. 4 SEM/EDS analyses of the Ti-6Al-4V/Ti_xC alloy after 5 h oxidation at 873 K: **a** and **b** SEM micrographs for TiC and Ti_2C; **c** a summary of principal element content in the tested regime

initio predictions that the Ti_2C phase is more favorable to be oxidized. It should also be noted that the Ti/C ratios of the tested regimes in Fig. 4a, b almost preserve the ideal values of 1 and 2, which evidences the reliability of the results.

In summary, the present work has addressed and examined a new insight into the role of the sub-stoichiometry in the oxidation kinetics of a δ-Ti_xC-doped Ti-based alloy. The major findings are summarized as follows:

(1) The ab initio simulation results indicate that owing to the sub-stoichiometric characteristic, the carbon-deficient Ti_2C exhibits a stronger oxidation propensity than TiC or α-Ti. This is attributed to the fact that oxygen occupancy is most energetically favored at the vacant carbon sites within Ti_2C.

(2) The proposed concept is successfully validated in a classical Ti-6Al-4V/Ti_xC alloy. It is observed that at 873 K, the δ-Ti_xC-doped Ti-6Al-4V alloy exhibits a much faster oxidation rate at the initial stage than its monolithic counterpart. The SEM/EDS analyses reveal that the oxygen content in Ti_2C is significantly higher than that in TiC or α-Ti, which further confirms the simulation results.

(3) A kinetic critical point is also observed during the oxidation process. It is found that the consumption of Ti_2C phase, the formation of localized passivation layer, and the refinement of oxide scale lead to the decreased oxidation rate of Ti-6Al-4V/Ti_xC alloy at extending oxidation time.

(4) In terms of high-temperature application of Ti_xC containing metallic or ceramic-based materials, the present findings suggest that pre-oxidation could be a potential approach to alleviate the negative effect of sub-stoichiometry-facilitated oxidation.

METHODS

Ab initio simulation

TiC (Fm-3m), Ti_2C (Fd3m), and α-Ti (P63/mmc) supercells each with 32 Ti atoms were constructed as illustrated in Fig. 1a, and were subsequently subjected to structural relaxation. Density functional theory simulations were performed by the Vienna Ab Initio Simulation Package,[34] and the generalized-gradient approximation in the Perdew-Burke-Ernzerhof form[35] was used for all calculations. For the three structures, it was found that a supercell consisting of 32 Ti atoms with a Monkhorst−Pack[36] k-point mesh of 9 × 9 × 9, an energy cutoff of 800 eV, and a maximum atomic force tolerance of 0.02 eV/Å are sufficient to reach converged acceptable precision. When performing ab initio molecular dynamics (MD) simulation at finite elevated temperatures, the same k-point mesh and an energy criterion of 1×10^{-5} eV were adopted to ensure high computational accuracy. All the MD simulations were conducted within an NVT ensemble at 873 K using a Nose-Hoover thermostat.[37] The simulations were performed with a time step of 1 fs until the total energy fluctuation was kept within 0.02 eV for at least 2 ps. The differential charge density (Δρ) of TiC, Ti_2C, and α-Ti each with one O atom incorporated was computed by $\Delta\rho = \rho_{with\ O} - (\rho_{without\ O} + \rho_{isolated\ O})$, where $\rho_{with\ O}$, $\rho_{without\ O}$, and $\rho_{isolated\ O}$ denote the charge density of the lattice with and without O atom, and an isolated O atom.

Alloy fabrication and characterization

Ti_xC particles with diameters of ~5 μm and a volume fraction of ~3.4% were doped into a high-purity Ti-6Al-4V alloy matrix (supporting information) via an in situ synthesis technique, of which the mechanisms have been demonstrated elsewhere.[38] To obtain a thermodynamically stable initial state, the bulk Ti-6Al-4V/Ti_xC specimens were subjected to high-vacuum (<10^{-4} Pa) furnace cool after being fabricated at 1473 K. Phase constitutions of the as-sintered alloys were analyzed using a Panalytical Empyrean XRD (scanning step 0.02°, four separate specimens were measured). An FEI Talos 200 TEM was employed to accomplish the crystallographic characterizations. Specimens for isothermal oxidation investigations were prepared following in the traditional metallographic routine. Oxidation kinetics was quantified by the conventional thermal gravity method at 873 K. At various oxidation states, the mass-gain values were monitored by a Mettler Toledo XPE205 analytical balance with precision secured to 0.01 mg. At least five specimens were weighted for each data point in order to avoid experimental occasionality and to ensure reproducibility. Surface morphologies of the oxidized samples were

investigated under a Zeiss SUPRA 55 SAPPHIR SEM equipped with an INCA 300 EDS and a Dimension Fastscan AFM.

DATA AVAILABILITY

All the data are available by contacting the corresponding authors of this work.

ACKNOWLEDGEMENTS

This work was financially supported by National Key R&D Program of China (No. 2017YFB0703100), National Natural Science Foundation of China under the grant numbers of 51822103, 51671068, and 51731009, and Fundamental Research Funds for the Central Universities (No. HIT.BRETIV.201902). The authors would like to extend their gratitude to Prof. Jane Dunphy, Prof. Wei Zhai, and Dr. Feng He for their critical suggestions on this work.

AUTHOR CONTRIBUTIONS

S.L.W. and L.J.H. conceived the project; S.L.W. led the experimental investigation; Z.S. and Y.Z. performed the ab initio simulation; X.T.L. participated in the alloy fabrication and structural characterization; S.L.W. and Y.Z. analyzed the data and wrote the paper; L.J.H. and L.G. supervised the research and contributed to the manuscript revision. All authors approved the final version of the manuscript.

ADDITIONAL INFORMATION

Supplementary information accompanies the paper on the *npj Materials Degradation* website (https://doi.org/10.1038/s41529-018-0067-9).

Competing interests: The authors declare no competing interests.

Publisher's note: Springer Nature remains neutral with regard to jurisdictional claims in published maps and institutional affiliations.

REFERENCES

1. Liu, A., Wentzcovitch, R. & Cohen, M. Structural and electronic properties of WC. *Phys. Rev. B* **38**, 9483–9489 (1988).
2. Karge, L. et al. The influence of C/Ta ratio on TaC precipitates in Co-Re base alloys investigated by small-angle neutron scattering. *Acta Mater.* **132**, 354–366 (2017).
3. Christensen, M., Wahnström, G., Allibert, C. & Lay, S. Quantitative analysis of WC grain shape in sintered WC-Co cemented carbides. *Phys. Rev. Lett.* **94**, 1–4 (2005).
4. Dy, L. C. & Williams, W. S. Resistivity, superconductivity, and order-disorder transformations in transition metal carbides and hydrogen-doped carbides. *J. Appl. Phys.* **53**, 8915–8927 (1982).
5. Price, L., Cooper, R., Virginia, W. & Wills, J. M. Carbon vacancies. *Phys. Rev. B* **48**, 311–315 (1993).
6. Riedl, H. et al. Influence of carbon deficiency on phase formation and thermal stability of super-hard TaC_y thin films. *Scr. Mater.* **149**, 150–154 (2018).
7. Pickett, W. E., Kleien, B. M. & Zeller, R. Electronic structure of the carbon vacancy in NbC. *Phys. Rev. B* **34**, 2517–2521 (1986).
8. Nakayama, H., Ozaki, K., Nabeta, T. & Nakajima, Y. Composition dependence of lattice parameter, thermal and electrical properties in ZrC_x Compounds. *Mater. Trans.* **58**, 852–856 (2017).
9. Zhang, Y., Liu, B., Wang, J. & Wang, J. Theoretical investigations of the effects of ordered carbon vacancies in ZrC_{1-x} on phase stability and thermo-mechanical properties. *Acta Mater.* **111**, 232–241 (2016).
10. Chen, P. H. & Nordlund, K. Modified embedded-atom method used to derive interatomic potentials for defects and phase formation in the W-C system. *Phys. Rev. B* **88**, 1–9 (2013).
11. Korzhavyi, P. A., Pourovskii, L. V., Hugosson, H. W., Ruban, A. V. & Johansson, B. Ab initio study of phase equilibria in TiC_x. *Phys. Rev. Lett.* **88**, 015505 (2001).
12. Eibler, R. New aspects of the energetics of ordered Ti_2C and Ti_2N. *J. Phys. Condens. Matter.* **19**, 19 (2007).
13. Music, D., Riley, D. P. & Schneider, J. M. Energetics of point defects in TiC. *J. Eur. Ceram. Soc.* **29**, 773–777 (2009).
14. Eibler, R. Electronic structure and energetics of ordered titanium carbides of composition Ti_2C. *J. Phys. Condens. Matter* **14**, 4425–4444 (2002).
15. Huang, L. J., Geng, L. & Peng, H. X. Microstructurally inhomogeneous composites: Is a homogeneous reinforcement distribution optimal? *Prog. Mater. Sci.* **71**, 93–168 (2015).
16. AlMangour, B., Grzesiak, D. & Yang, J. M. In situ formation of TiC-particle-reinforced stainless steel matrix nanocomposites during ball milling: Feedstock powder preparation for selective laser melting at various energy densities. *Powder Technol.* **326**, 467–478 (2018).
17. Miyamoto, S. et al. Phase equilibria, microstructure, and high-temperature strength of TiC-added Mo-Si-B alloys. *Metall. Mater. Trans. A* **45**, 1112–1123 (2014).
18. Li, M. et al. Microstructure and mechanical properties of $TiC_{0.5}$ reinforced copper matrix composites. *Mater. Sci. Eng. A* **588**, 335–339 (2013).
19. Létiche, M. et al. Sputtered titanium carbide thick film for high areal energy on chip carbon-based micro-supercapacitors. *Adv. Funct. Mater.* **27**, 1606813(1–10) (2017).
20. Back, S. & Jung, Y. TiC- and TiN-supported single-atom catalysts for dramatic improvements in CO_2 electrochemical reduction to CH_4. *ACS Energy Lett.* **2**, 969–975 (2017).
21. Molina-Jordá, J. M. Mesophase pitch-derived graphite foams with selective distribution of TiC nanoparticles for catalytic applications. *Carbon N. Y.* **103**, 5–8 (2016).
22. Park, H. U., Lee, E. & Kwon, Y. U. TiC supported Pt-based nanoparticles: Facile sonochemical synthesis and electrocatalytic properties for methanol oxidation reaction. *Int. J. Hydrog. Energy* **42**, 19885–19893 (2017).
23. Lavrenko, V. A., Glebov, L. A., Pomitkin, A. P., Chuprina, V. G. & Protsenko, T. G. High-temperature oxidation of titanium carbide in oxygen. *Oxid. Met.* **9**, 171–179 (1975).
24. Qin, Y., Lu, W., Zhang, D., Qin, J. & Ji, B. Oxidation of in situ synthesized TiC particle-reinforced titanium matrix composites. *Mater. Sci. Eng. A* **404**, 42–48 (2005).
25. Saunders, S. R. J., Monteiro, M. & Rizzo, F. The oxidation behaviour of metals and alloys at high temperatures in atmospheres containing water vapour: a review. *Prog. Mater. Sci.* **53**, 775–837 (2008).
26. Li, X. T. et al. Cycle oxidation behavior and anti-oxidation mechanism of hot-dipped aluminum coating on TiBw/Ti6Al4V composites with network microstructure. *Sci. Rep.* **8**, 5790 (2018).
27. Guleryuz, H. & Cimenoglu, H. Oxidation of Ti-6Al-4V alloy. *J. Alloys Compd.* **472**, 241–246 (2009).
28. Vasylyev, M. A., Chenakin, S. P. & Yatsenko, L. F. Ultrasonic impact treatment induced oxidation of Ti6Al4V alloy. *Acta Mater.* **103**, 761–774 (2016).
29. Qin, Y. X., Zhang, D., Lu, W. J. & Pan, W. Oxidation behavior of in situ-synthesized (TiB+TiC)/Ti6242 composites. *Oxid. Met.* **66**, 253–268 (2006).
30. Song, M. H., Han, S. M., Min, D. J., Choi, G. S. & Park, J. H. Diffusion of oxygen in β-titanium. *Scr. Mater.* **59**, 623–626 (2008).
31. Wu, H. H. & Trinkle, D. R. Direct diffusion through interpenetrating networks: oxygen in titanium. *Phys. Rev. Lett.* **107**, 1–4 (2011).
32. Liu, F. et al. Preparation of Ti_3C_2 and Ti_2C MXenes by fluoride salts etching and methane adsorptive properties. *Appl. Surf. Sci.* **416**, 781–789 (2017).
33. Bursik, J. & Weatherly, G.C. Ordering of Substoichiometric δ-TiC_x Phase in Ti-V-C Alloys. *Phys. Stat. Solid A* **327**, 327–336 (1999).
34. Kresse, G. & Furthmüller, J. Efficient iterative schemes for ab initio total-energy calculations using a plane-wave basis set. *Phys. Rev. B - Condens. Matter* **54**, 11169–11186 (1996).
35. Perdew, J. P., Burke, K. & Ernzerhof, M. Generalized gradient approximation made simple- ERRATA. *Phys. Rev. Lett.* **77**, 3865–3868 (1997).
36. Pack, J. D. & Monkhorst, H. J. 'special points for Brillouin-zone integrations'-a reply. *Phys. Rev. B* **16**, 1748–1749 (1977).
37. Nosé, S. Constant temperature molecular dynamics methods limitations in simulations in the microcanonical ensemble. *Prog. Theor. Phys. Suppl. 103*, 1 (1991).
38. Wei, S. L., Huang, L. J., Li, X. T., An, Q. & Geng, L. Interactive effects of cyclic oxidation and structural evolution for Ti-6Al-4V /(TiC+TiB) alloy composites at elevated temperatures. *J. Alloys Compd.* **752**, 164–178 (2018).